Structure, Magnetism, and Substitutional Chemistry of Cation-Ordered $(Ba/Sr)_{5+n}Mn_{3+n}Cr_2O_{3n+14}$ Phases

Joanna H. Clark and Michael A. Hayward*

Department of Chemistry, Inorganic Chemistry Laboratory, University of Oxford, South Parks Road, Oxford, OX1 3QR

Received February 21, 2008. Revised Manuscript Received May 8, 2008

The synthesis and characterization of $(Ba_{0.5}Sr_{0.5})_6Mn_4Cr_2O_{17}$ is reported. Neutron powder diffraction data reveal a hexagonal perovskite structure based on a 12H stacking sequence ($P6_3/mmc$, $a = 5.6232(7)$ Å, $c = 28.201(4)$ Å) with an ordered array of Cr^V, Mn^{IV}, and Mn^{II} centers. Low-temperature neutron powder diffraction data collected from the related phase $Ba_7Mn_5Cr_2O_{20}$ reveal 2D magnetic order below 50 K, which can be transformed into 3D order on application of a magnetic field. Chemical substitution of diamagnetic Ca^{II} and V^V centers into the material to form phases of composition $Ba_7Ca_2Mn_3Cr_2O_{20}$ and $Ba_7Ca_2Mn_3V_2O_{20}$ reveals that strong antiferromagnetic coupling exists between Mn^{IV} centers even at room temperature.

Introduction

The preparation of phases with ordered arrays of two or more transition-metal cations is a longstanding goal in solid-state synthesis due to the properties such phases could offer. Typically the thermodynamic competition between different possible structures or cation ordering schemes is dominated by entropy, and thus, statistically disordered structures are strongly favored. To overcome this entropy driven thermodynamic preference for formation of disordered structures a strong enthalpic drive favoring formation of ordered structures must be provided. A suitable enthalpic drive can be provided by a large difference in size and/or charge between the cations to be ordered as ordered structures lower the lattice strain of such systems relative to disordered structures. This strategy has been used effectively in the preparation of cubic double perovskites such as the $Sr_2MoB'O_6$ ($B' =$ Mn, Fe, Co, Ni) series, for example.[1–3] A similar approach can be applied to the hexagonal perovskite structural series. When large cations, such as barium, combine with transition metals to form complex oxide phases the structures adopted incorporate face sharing of MO_6 transition-metal−oxygen octahedra into the apex-linked MO_6 network present in cubic perovskites.[4] The resulting hexagonal perovskite structural series can provide a wide variety of coordination sites for transition metals and other small cations. These different sites can in principle be used to differentiate between different cations on the basis of charge and size, resulting in formation of ordered cation lattices such as those seen in $Ba_3MRu_2O_9$ ($M =$ Co, Ni, Fe)[5] or Ba_2CrNbO_6.[6]

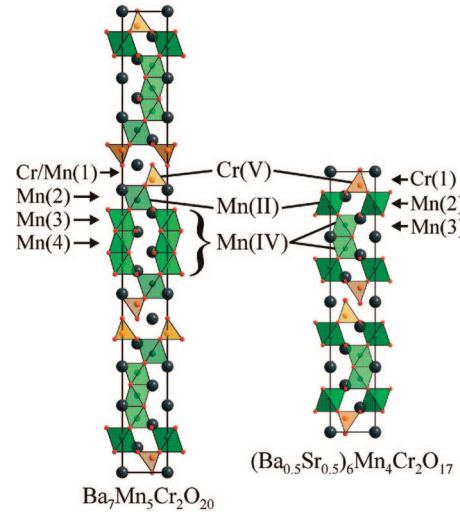

Figure 1. Structures of (a) $Ba_7Mn_5Cr_2O_{20}$ and (b) $(Ba_{0.5}Sr_{0.5})_6Mn_4Cr_2O_{17}$ exhibiting chemical and charge order.

Recently we reported the preparation of $Ba_7Mn_5Cr_2O_{20}$[7] which has a structure based on the hexagonal perovskite series with a basic structural framework that has three very different transition-metal coordination sites: tetrahedral, apex-sharing octahedral, and face-sharing octahedral (Figure 1). As noted above, these sites can readily differentiate between transition-metal cations on the basis of size and charge, leading to both the chemical ordering of chromium and manganese ions and disproportionation of the manganese oxidation state into a charge-ordered array of Mn^{II} and Mn^{IV} centers. Here we report the study of the substitutional

* To whom correspondence should be addressed. Phone: +44 1865 272623. Fax: +44 1865 272690. E-mail: michael.hayward@chem.ox.ac.uk.

(1) Kobayashi, K. L.; Kimura, T.; Sawada, H.; Terakura, K.; Tokura, Y. *Nature* **1998**, *395*, 677.
(2) Munoz, A.; Alonso, J. A.; Casais, M. T.; Martinez-Lope, M. J.; Fernandez-Diaz, M. T. *J. Phys.:Condens. Matter* **2002**, *14*, 8817.
(3) Gagulin, W.; Korchagina, S. K.; Ivanova, W.; Shevxhuk, Y. A. *Inorg. Mater.* **2003**, *39*, 625.
(4) Darriet, J.; Subramanian, M. A. *J. Mater. Chem.* **1995**, *5*, 543.
(5) Rijssenbeek, J. T.; Huang, Q.; Erwin, R. W.; Zandbergen, H. W.; Cava, R. J. J. *Solid State Chem.* **1999**, *146*, 65.
(6) Choy, J.; Hong, S.; Choi, K. *J. Chem. Soc., Faraday Trans.* **1996**, *92*, 1051.
(7) Dunstone, S. J.; Clark, J. H.; Hayward, M. A. *Chem. Commun.* **2007**, *19*, 1905.

10.1021/cm8005138 CCC: $40.75
Published on Web 06/18/2008

chemistry and complex magnetic behavior of $Ba_7Mn_5Cr_2O_{20}$ and related phases.

Experimental Section

Samples of composition $(Ba_{1-x}Sr_x)_7Mn_5Cr_2O_{21-\hat{y}}$ ($0 < x < 0.5$) were prepared from suitable molar ratios of $BaCO_3$ (99.997%), $SrCO_3$ (99.994%), MnO_2 (99.995%), and Cr_2O_3 (99.995%). After being thoroughly mixed in an agate pestle and mortar the samples were heated at 1000 °C in air for 24 h and then pressed into 13 mm pellets. Samples were then heated at 1250 °C under flowing argon for seven periods of 40 h with regrinding between heating periods. Large samples (~3 g) of $Ba_7Mn_5Cr_2O_{20}$ and $(Ba_{0.5}Sr_{0.5})_6Mn_4Cr_2O_{17}$ suitable for neutron diffraction measurements were prepared as described above.

In order to isolate the different magnetic centers in the structure of $Ba_7Mn_5Cr_2O_{20}$, samples doped with diamagnetic Ca^{II} and V^V ions were prepared as described above but for the substitution of suitable quantities of $CaCO_3$ (99.999%) for MnO_2 and V_2O_5 (99.995%) for Cr_2O_3 resulting in samples of composition $Ba_7Ca_2Mn_3Cr_2O_{20}$ and $Ba_7Ca_2Mn_3V_2O_{20}$.

Powder X-ray diffraction data were collected using a PANalytical X'Pert diffractometer incorporating an X'celerator position-sensitive detector (monochromatic Cu Kα1 radiation). Neutron powder diffraction data were collected using the D2B diffractometer at the ILL neutron source, Grenoble. Rietveld refinement of diffraction data was performed utilizing the GSAS suite of programs.[8] Diffraction data were collected from samples of $Ba_7Mn_5Cr_2O_{20}$ and $(Ba_{0.5}Sr_{0.5})_6Mn_4Cr_2O_{17}$ at 298 and 5 K using a neutron wavelength of 1.59 Å. In addition, data were also collected from both samples at 5 K in a cryomagnet with a neutron wavelength of 2.4 Å. Initially measurements were performed in zero applied field and then in an applied field of 60 KOe after cooling in the measuring field. In order to minimize any preferred orientation effects caused by reorientation of particles on application of the magnetic field, the powder samples were tightly packed into vanadium cans. In addition, after measurements in applied fields had been completed, a final set of diffraction data was collected at 5 K after cooling in zero field to quantify any preferred orientation which had been induced. The zero-field data sets collected before and after the applied field measurements were identical within error for both samples, and so preferred orientation effects were omitted from subsequent data analysis. Zero-field-cooled and field-cooled magnetization data were collected as a function of temperature in an applied field of 100 Oe from powder samples with an approximate mass of 50 mg using a Quantum Design MPMS SQUID magnetometer. In addition, magnetization-field isotherms were collected between ±50 KOe from samples at 5 K. The average oxidation states of transition metals were determined by dissolving samples in dilute HCl containing an excess of KI and titrating the liberated I_2 with $Na_2S_2O_3$.

Results

Structural Characterization. X-ray powder diffraction data collected from samples of composition $(Ba_{1-x}Sr_x)_7Mn_5Cr_2O_{20}$, $0 < x < 0.3$, could be readily indexed on the basis of the rhombohedral unit cells detailed in Table 1. Rietveld refinement of the seven-layer model previously reported for $Ba_7Mn_5Cr_2O_{20}$[7] against these data confirmed the simple substitution of strontium for barium had occurred.

Table 1. Lattice Parameters for Phases with the Seven-Layer Structure

phase $(Ba_{1-x}Sr_x)_7Mn_5Cr_2O_{20}$	x	*a*(Å)	*c*(Å)
	0	5.7401(1)	50.597(1)
	0.1	5.7207(1)	50.298(1)
	0.2	5.7018(1)	50.044(1)
	0.3	5.6764(2)	49.697(3)
$Ba_7Ca_2Mn_3Cr_2O_{20}$		5.8278(1)	51.356 (1)
$Ba_7Ca_2Mn_3V_2O_{20}$		5.8309(1)	51.393(1)

X-ray powder diffraction data collected from a sample of composition $(Ba_{0.6}Sr_{0.4})_7Mn_5Cr_2O_{21-x}$ contained evidence for a second hexagonal phase with a six-layer stacking sequence in addition to the seven-layer phase. This six-layer phase was observed to be the only phase present (along with 4H-(Ba/Sr)MnO_{3-x}[9]) in a sample of $(Ba_{0.5}Sr_{0.5})_7Mn_5Cr_2O_{21-x}$, suggesting it had a composition of $(Ba_{0.5}Sr_{0.5})_6Mn_4Cr_2O_{17}$; a sample of this composition was subsequently prepared as described above.

X-ray and neutron powder diffraction data collected from $(Ba_{0.5}Sr_{0.5})_6Mn_4Cr_2O_{17}$ could be readily indexed on the basis of a hexagonal unit cell, $a = 5.6232(7)$ Å, $c = 28.20(4)$ Å, and were consistent with the $P6_3/mmc$ space group. By analogy with the structure of $Ba_7Mn_5Cr_2O_{20}$ (Figure 1a) this suggested a six-layer structure with a *hccccc* stacking sequence as shown in Figure 1b. This model corresponds to the $n = 1$ member of the $A_{5+n}Mn_{3+n}Cr_2O_{3n+14}$ series of which $Ba_7Mn_5Cr_2O_{20}$ is the $n = 2$ member. Refinement of this model against neutron powder diffraction data collected at room temperature gave a relatively good fit ($\chi^2 = 2.2$) There were however a number of weak reflections which could not be accounted for by the model. These were assigned to the presence of a small quantity of 4H-(Ba/Sr)MnO_{3-x}.[9] This was added to the model as a second phase with an associated improvement to the goodness of fit parameters. The Ba/Sr ratio of each of the four A-cation sites was refined with the overall Ba/Sr ratio of the phase constrained to be unity. The fractional occupancy of the manganese and chromium sites was refined to check for anti-site disorder. No B-cation anti-site disorder was observed within error (in contrast to $Ba_7Mn_5Cr_2O_{20}$[7]), so a fully ordered model was retained. In the final refinement cycles the positional parameters and displacement factors of all atoms were refined. Complete structural details are given in Table 2 with selected bond lengths in Table 3. A comparison of the observed and calculated diffraction data is shown in Figure 2.

X-ray powder diffraction data collected from $Ba_7Ca_2Mn_3Cr_2O_{20}$ and $Ba_7Ca_2Mn_3V_2O_{20}$ could be readily indexed on the basis of the rhombohedral unit cells in Table 1, consistent with the $Ba_7Mn_5Cr_2O_{20}$ parent structure. The lattice expansion on substitution of Mn^{II} by Ca^{II} is consistent with the ionic radii of the two metals ($Mn^{II} = 0.83$Å, $Ca^{II} = 1.00$ Å[10]); likewise the smaller expansion on substitution of Cr^V by V^V is also consistent with the ionic radii ($Cr^V = 0.345$Å, $V^V = 0.355$ Å[10]). Considering the ionic radii of Ca^{II} and V^V and the reported cation distributions in the structur-

(8) Larson, A. C.; Von Dreele, R. B. *General Structure Analysis System*; Los Alamos National Laboratory Report LAUR 86-748, 2000.

(9) Adkin, J. J.; Hayward, M. A. J. *Solid State Chem.* **2006**, *179*, 70.

(10) Shannon, R. D. *Acta Crystallogr.* **1976**, *A32*, 751.

Table 2. Refined Strucutral Parameters for $(Ba_{0.5}Sr_{0.5})_6Mn_4Cr_2O_{17}$

atom		*x*	*y*	*z*	fraction	U_{iso}
Ba/Sr(1)	2a	0	0	0.5	0.76(1)/0.24(1)	0.004(1)
Ba/Sr(2)	4f	0.667	0.333	0.5944(3)	0.22(1)/0.78(1)	0.004(1)
Ba/Sr(3)	4f	0.333	0.667	0.6799(3)	0.59(1)/0.41(1)	0.004(1)
Ba/Sr(4)	2b	0	0	0.75	0.62(1)/0.38(1)	0.004(1)
Mn(1)	4f	0.667	0.333	0.7048(4)	1	0.005(1)
Mn(2)	4e	0	0	0.6313(6)	1	0.006(1)
Cr(1)	24l	0.333	0.667	0.5534(7)	1	0.013(2)
O(1)	6h	0.5143(7)	0.028(1)	0.75	1	0.002(1)
O(2)	12k	0.8308(8)	0.1691(8)	0.6664(1)	1	0.002(1)
O(3)	24l	0.167(1)	0.832(1)	0.5790(2)	1	0.002(1)
O(4)	12k	0.333	0.667	0.4942(7)	1	0.010(2)

[a] Space group = *P*63/*mmc*, a = 5.6232(7) Å, c = 28.201(4) Å. 4H−$Ba_{0.5}Sr_{0.5}MnO_{3-x}$, a = 5.5932(8) Å, c = 9.283(2) Å. Mole fraction = 8.1(8)%, χ^2 = 1.43, wR_p = 6.13%, R_p = 4.80%.

Table 3. Selected Bonds Lengths for $(Ba_{0.5}Sr_{0.5})_6Mn_4Cr_2O_{17}$

cation	anion	bond length (Å)	BVS
Mn(1)	O(1)	1.959(8) × 3	3.641
	O(2)	1.931(7) × 3	
Mn(2)	O(2)	1.92(1) × 3	2.88
	O(3)	2.19(1) × 3	
Cr(1)	O(3)	1.76(1) × 3	
	O(4)	1.66(2) × 1	
Ba(1)	O(3)	2.761(6) × 6	
	O(4)	3.251(1) × 6	
Ba(2)	O(2)	2.585(7) × 3	
	O(3)	2.842(6) × 6	
	O(4)	2.49(2) × 1	
Ba(3)	O(1)	2.647(7) × 3	
	O(2)	2.837(5) × 6	
	O(3)	3.272(9) × 3	
Ba(4)	O(1)	2.817(3) × 6	
	O(2)	2.876(2) × 6	

ally analogous phases $Ba_7Ca_2Mn_5O_{20}$ and $Ba_8Ca_2Mn_6O_{23}$[11,12] the most chemically reasonable site to locate Ca^{II} is Mn(2) and V^V is Cr/Mn(1) as shown in Figure 1. Structural models based on the structure of $Ba_7Mn_5Cr_2O_{20}$ with these cation substitutions were refined against X-ray powder diffraction data collected from samples of $Ba_7Ca_2Mn_3Cr_2O_{20}$ and $Ba_7Ca_2Mn_3V_2O_{20}$. Good agreement was achieved between observed and calculated diffraction patterns for both samples; however, in the case of the vanadium-doped sample, $Ba_3V_2O_8$[13] had to be added as a second phase to achieve a good statistical fit. Full details of both structural refinements are given in the Supporting Information. Iodometric titration data were consistent with the presence of $3Mn^{IV}$ and $2Cr^V$ for $Ba_7Ca_2Mn_3Cr_2O_{20}$ and with $3Mn^{IV}$ for $Ba_7Ca_2Mn_3V_2O_{20}$, consistent with the assignment of the cation distribution.

Magnetic Characterization. Magnetization data collected from $Ba_7Mn_5Cr_2O_{20}$ could be fitted by the Curie−Weiss law in the range 100 < *T*/K < 300 as shown in Figure 3a. Below this temperature there is a sharp rise in the magnetization at ~50 K. Magnetization field isotherms collected at 5 K are suggestive of ferromagnetic order (Figure 4a).

In order to investigate the magnetic order present in $Ba_7Mn_5Cr_2O_{20}$ low-temperature neutron powder diffraction data were collected. Surprisingly, data collected at 5 K in zero applied field showed no evidence of additional magnetic

(11) Floros, N.; Michel, C.; Hervieu, M.; Raveau, B. J. *Solid State Chem.* **2002**, *168*, 11.
(12) Floros, N.; Michel, C.; Hervieu, M.; Raveau, B. *Chem. Mater.* **2000**, *12*, 3197.
(13) Liu, G.; Greedan, J. E. J. *Solid State Chem.* **1994**, *110*, 274.

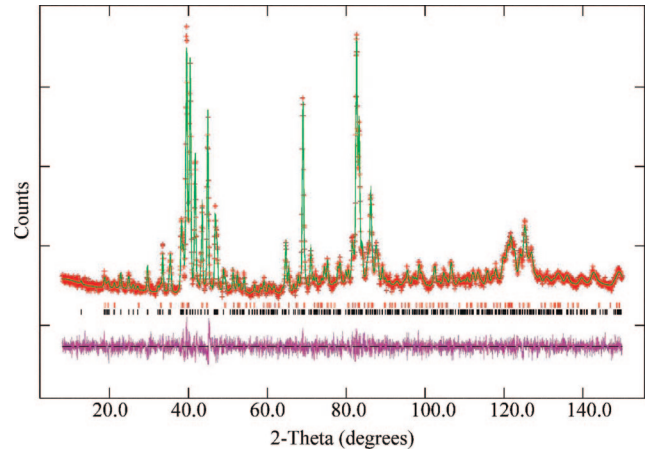

Figure 2. Observed calculated and difference plots from the structural refinement of $(Ba_{0.5}Sr_{0.5})_6Mn_4Cr_2O_{17}$ against neutron powder diffraction data collected at room temperature. Lower tick marks indicate reflection positions of the majority phase and upper tick mark those of a (Ba/Sr)MnO_{3-x} impurity.

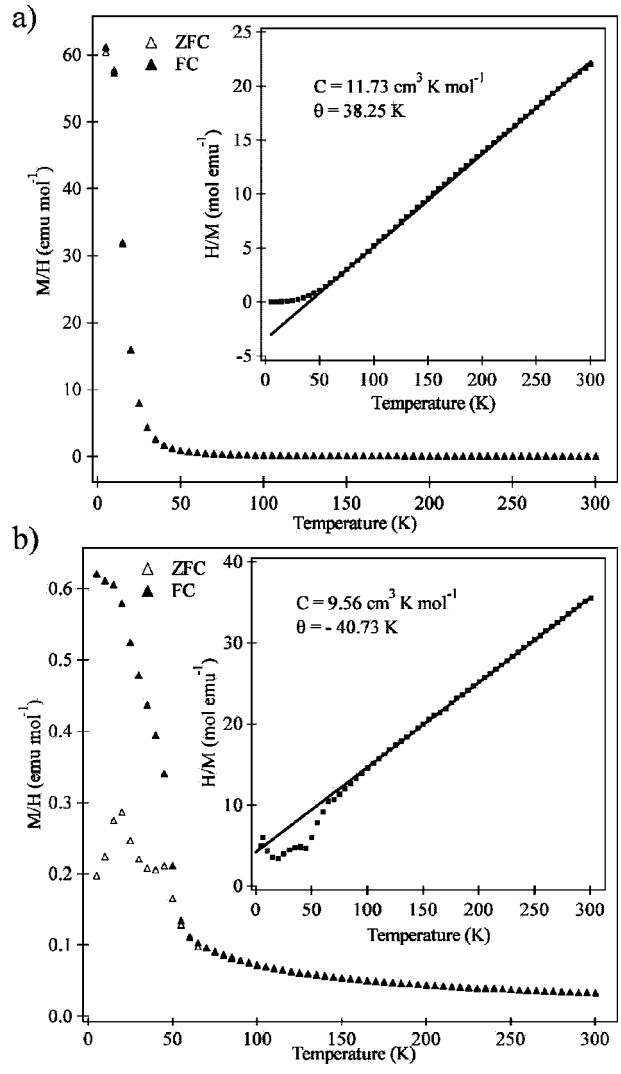

Figure 3. Zero-field-cooled and field-cooled magnetization data collected from (a) $Ba_7Mn_5Cr_2O_{20}$ and (b) $(Ba_{0.5}Sr_{0.5})_6Mn_4Cr_2O_{17}$. Insets show linear fits of H/M against temperature consistent with the Curie−Weiss law.

Bragg peaks. All the sharp diffraction features could be accounted for completely by a nuclear only model. Close

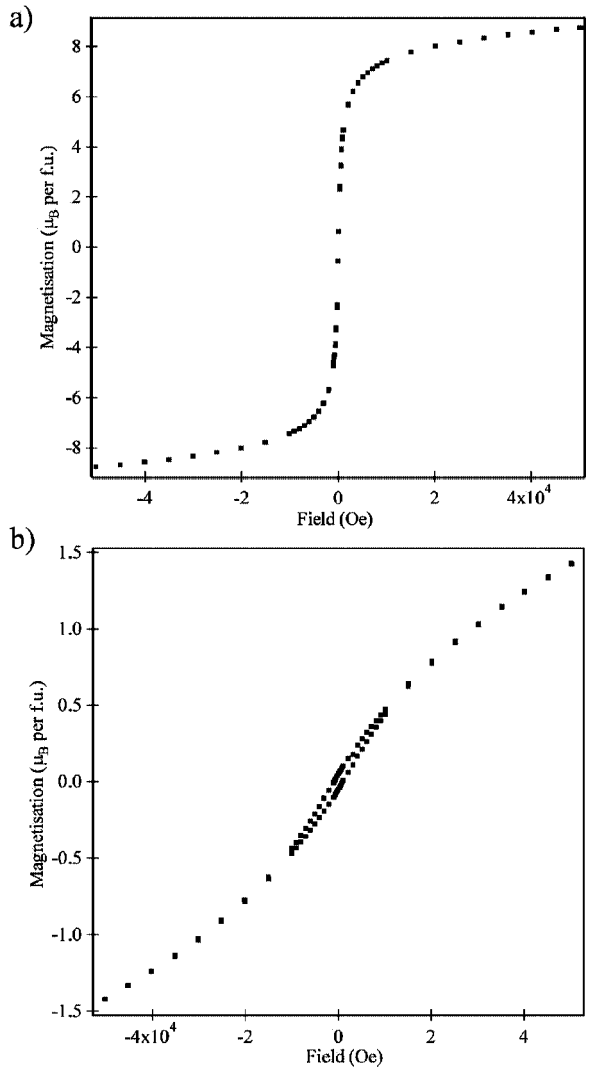

Figure 4. Magnetization-field isotherms collected at 5 K from (a) $Ba_7Mn_5Cr_2O_{20}$ and (b) $(Ba_{0.5}Sr_{0.5})_6Mn_4Cr_2O_{17}$.

examination of the fit to the data collected at 5 K however revealed broad, weak diffraction features centered on the Bragg peaks (Figure 5). These features are most noticeable as broad lumps in the difference plot of the fit to the 5 K data centered approximately at 25° and 10° 2θ. It can also be seen that the significant rise in the background of the 298 K data at low 2θ, associated with paramagnetic scattering, has diminished in the 5 K data. These features together are suggestive of the onset of short-range magnetic order at low temperature.

To investigate the magnetic behavior of $Ba_7Mn_5Cr_2O_{20}$ further neutron powder diffraction data were collected at 5 K in an applied field of 60 KOe (sample cooled in measuring field). These data exhibit significant changes in the intensity of some low-angle Bragg peaks relative to the zero-field data (Figure 6). These additional features could be indexed on the basis of the nuclear cell. The magnetic model shown in Figure 7 was refined against the data and found to fit well. A comparison of the fit to the data for the nuclear only (0 Oe) and nuclear and magnetic models (60 KOe) are shown in Figure 6. Full details of the refined magnetic model are given in the Supporting Information.

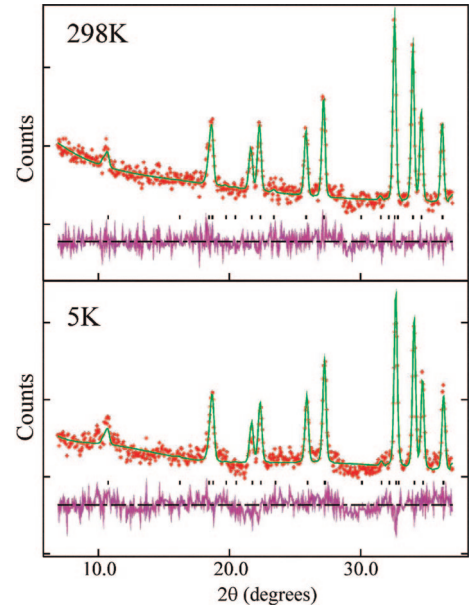

Figure 5. Observed calculated and difference plots from the refinement of nuclear only $Ba_7Mn_5Cr_2O_{20}$ models against neutron powder diffraction data collected at 298 and 5 K.

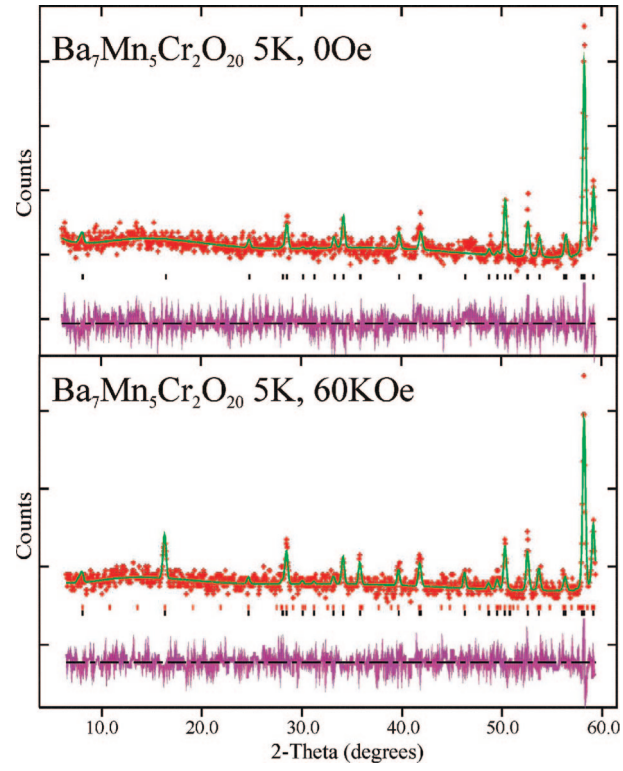

Figure 6. Observed calculated and difference plots from the refinement of a nuclear only model (0 Oe) and a nuclear and magnetic model (60 KOe) against neutron powder diffraction data collected from $Ba_7Mn_5Cr_2O_{20}$ at 5 K.

Magnetization data collected from $(Ba_{0.5}Sr_{0.5})_6Mn_4Cr_2O_{17}$, like that of $Ba_7Mn_5Cr_2O_{20}$, could also be fitted to the Curie−Weiss law (Figure 3b). These data also showed a sharp rise at 50 K; however, the magnitude of the low-temperature data and the form of the 5 K magnetization-field isotherm are suggestive of canted antiferromagnetic behavior rather than the ferromagnetic behavior observed for

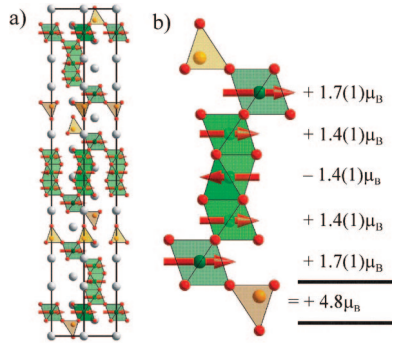

Figure 7. Magnetic model refined from neutron powder diffraction data for $Ba_7Mn_5Cr_2O_{20}$ in an applied field of 60 KOe.

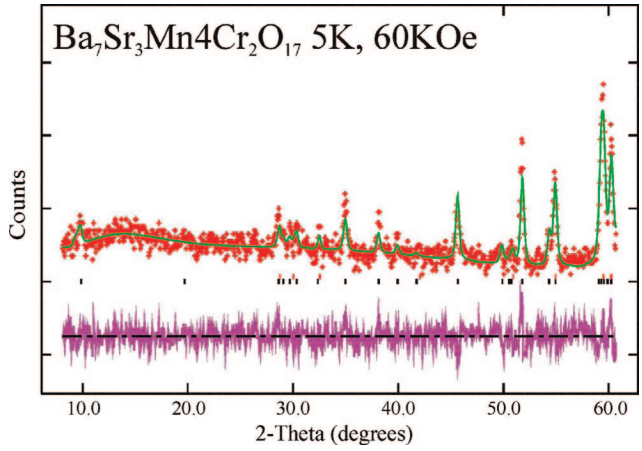

Figure 8. Observed calculated and difference plots from the refinement of a nuclear only model of $(Ba_{0.5}Sr_{0.5})_6Mn_4Cr_2O_{17}$ against neutron powder diffraction data collected at 5 K in an applied field of 60 KOe.

$Ba_7Mn_5Cr_2O_{20}$ (Figure 4b). Low-temperature (5 K) neutron diffraction data collected from $(Ba_{0.5}Sr_{0.5})_6Mn_4Cr_2O_{17}$ either in zero field or in an applied field of 60 KOe showed no evidence of additional magnetic diffraction features and could be fitted effectively by a nuclear only model. The fit to the 5 K data collected in a 60 KOe field (after cooling in the field) are shown in Figure 8.

Magnetization data collected from $Ba_7Ca_2Mn_3Cr_2O_{20}$ and $Ba_7Ca_2Mn_3V_2O_{20}$ are paramagnetic over the entire measured temperature range ($5 < T/K < 300$) (Figure 9).

Discussion

Structural Effects. Inspection of the structure refined for $(Ba_{0.5}Sr_{0.5})_6Mn_4Cr_2O_{17}$ (Tables 2 and 3) and comparison with the structural parameters refined for $Ba_7Mn_5Cr_2O_{20}$[7] reveals the Ba/Sr A-cation sites in the former phase are significantly smaller than the analogous sites in the seven-layer structure consistent with substitution of the smaller Sr^{II} for Ba^{II}. The group 2 cations are distributed with the large Ba^{II} predominantly in the large coordination sites and the Sr^{II} in the smaller sites.

The relative proportions of hexagonal and cubic stacking in the structures of hexagonal perovskites is determined by the structural tolerance factor, t ($t = \langle A{-}O\rangle/\sqrt{2}\ \langle B{-}O\rangle$). Large values favor hexagonal stacking, with small values favoring cubic stacking. The reduction in the average A-cation size by substituting Sr^{II} for Ba^{II} can therefore be

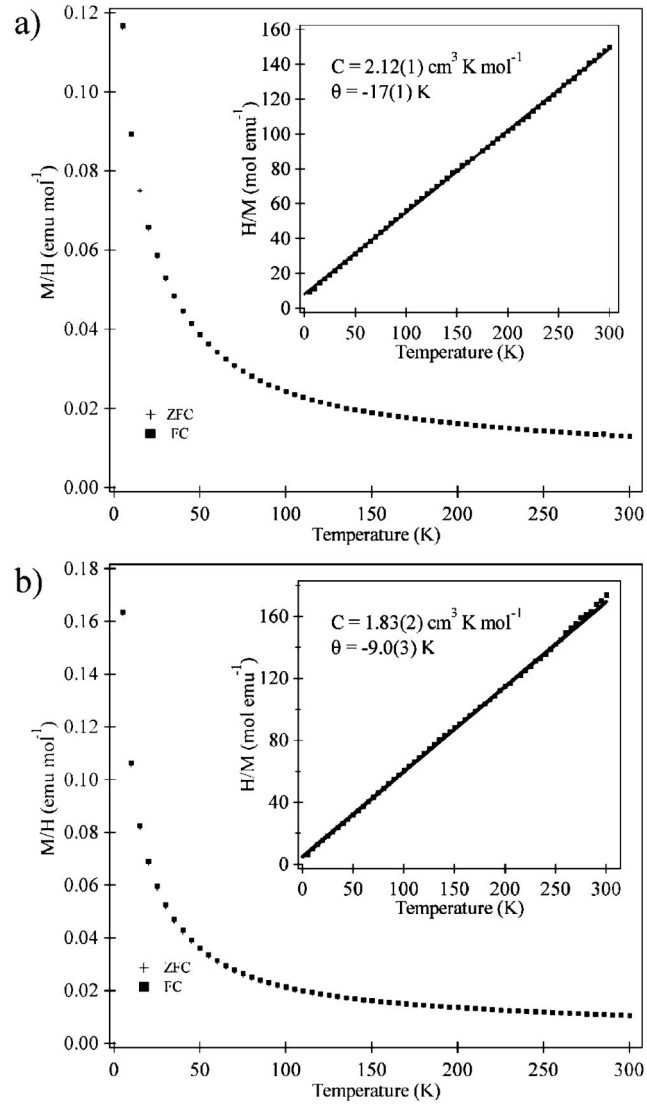

Figure 9. Zero-field-cooled and field-cooled magnetization data collected from (a) $Ba_7Ca_2Mn_3Cr_2O_{20}$ and (b) $Ba_7Ca_2Mn_3V_2O_{20}$. Insets show linear fits of H/M against temperature consistent with the Curie–Weiss law.

seen as the driving force for the change from the seven-layer *hhccccc* structure to the six-layer *hccccc* structure as confirmed by the tolerance factors of $Ba_7Mn_5Cr_2O_{20}$ (2.961Å/($\sqrt{2}$ × 1.948Å) = 1.074) and $(Ba_{0.5}Sr_{0.5})_6Mn_4Cr_2O_{17}$ (2.87Å/($\sqrt{2}$ × 1.933Å) = 1.051). The co-existence of both the seven- and the six-layer phases in the sample of composition $(Ba_{0.6}Sr_{0.4})_7Mn_5Cr_2O_{21-x}$ demonstrates the Mn:Cr ratio of a sample does not have a significant influence on determining the structure adopted. This is in contrast to the structurally analogous $Ba_{5+n}Mn_{3+n}Ca_2O_{3n+14}$ series in which the Mn:Ca ratio differentiates between the $n = 2$ and 3 members.[11,12] It is assumed that the rigidity of the Ca^{II} oxidation state in contrast to the relative ease of oxidation of Mn^{II} leads to this difference. The striking disproportionation of the manganese oxidation state into Mn^{II} and Mn^{IV} observed for $Ba_7Mn_5Cr_2O_{20}$ is less dramatic for $(Ba_{0.5}Sr_{0.5})_6Mn_4Cr_2O_{17}$. Bond valence sums[14] calculated for the two manganese sites give values of Mn(3) = +3.64 and Mn(2)= +2.88 relative

(14) Brese, N. E.; O'Keefe, M. *Acta Crystallogr., Sect. B: Struct. Sci.* **1991**, *B47*, 192–197.

to the average manganese oxidation state of +3. This could in part be due to the general contraction of the crystal lattice on strontium substitution and/or indicate a less rigorous charge ordering in the six-layer material, although this would contradict the magnetic data.

The structural data refined for $Ba_7Ca_2Mn_3Cr_2O_{20}$ and $Ba_7Ca_2Mn_2V_2O_{20}$ are consistent with the simple substitution of Ca^{II} and V^{V} into the structure of $Ba_7Mn_5Cr_2O_{20}$. The similarity of the scattering powers of calcium, vanadium, chromium, and manganese make it impossible to rigorously determine the cation distributions in these phases with X-ray diffraction data. However, on the grounds of chemical reasonability and consistency with the titration data, we propose that Ca^{II} replaces Mn^{II} in the large apex-linked octahedral site (Mn(2)) and that V^{V} replaces Cr^{V} in the tetrahedral site (Mn(1)). We will use this as a working assumption for treatment of the magnetic data.

Magnetism. The magnetization data collected as a function of temperature from both $Ba_7Mn_5Cr_2O_{20}$ and $(Ba_{0.5}Sr_{0.5})_6Mn_4Cr_2O_{17}$ are consistent with the Curie−Weiss law (Figure 3). The moments extracted for both phases from plots of $1/\chi$ against temperature are much smaller than would be expected from the simple addition of squares of the spin-only moments [$Ba_7Mn_5Cr_2O_{20}$: $C_{expected} = 15.12$ cm^3 K mol^{-1}, $C_{obs} = 11.73$ cm^3 K mol^{-1}; $(Ba_{0.5}Sr_{0.5})_6Mn_4Cr_2O_{17}$: $C_{expected} = 13.25$ cm^3 K mol^{-1}, $C_{obs} = 9.56$ cm^3 K mol^{-1}]. Studies of hexagonal perovskite phases containing manganese ions (e.g., 4H-$SrMnO_3$ and the $BaMnO_{3-x}$ series[15,16]) have revealed strong room-temperature antiferromagnetic coupling between manganese centers in chains of face-sharing MnO_6 octahedra. If an analogous strong coupling were to occur between the manganese centers linked by the face-sharing MnO_6 octahedra in $(Ba_{0.5}Sr_{0.5})_6Mn_4Cr_2O_{17}$ only the magnetic susceptibility of the Cr^{IV} and Mn^{II} centers would be observed. This would yield a $C_{expected} = 9.50$ cm^3 K mol, in good agreement with the observed value of 9.56 cm^3 K mol^{-1}, providing support for the disproportionation of the manganese oxidation state into Mn^{II} on site Mn(2) and Mn^{IV} on site Mn(3).

The magnetization data collected from $Ba_7Ca_2Mn_3V_2O_{20}$ suggest a similar coupling exists between the Mn^{IV} centers in the trimer of face-sharing MnO_6 octahedra. Fits to the Curie−Weiss law in the temperature range $5 < T/K < 300$ yield a Curie constant of 1.83 cm^3 K mol^{-1}, close to the value of 1.87 cm^3 K mol^{-1} expected from a single $S = 3/2$ Mn^{IV} center. This suggests an antiferromagnetically coupled trimer exists in which the spins on two of the three manganese centers 'cancel', resulting in a unit which behaves as a single $S = 3/2$ center. The paramagnetic moments of $Ba_7Mn_5Cr_2O_{20}$ and $Ba_7Ca_2Mn_3Cr_2O_{20}$ are similarly reduced, although they do not show as close a match to the values expected if the moment from only one of the three Mn^{IV} centers is observed ($Ba_7Mn_5Cr_2O_{20}$: $C_{exp} = 11.37$ cm^3 K mol^{-1}, $C_{obs} = 11.73$ cm^3 K mol^{-1}; $Ba_7Ca_2Mn_3Cr_2O_{20}$: $C_{exp} = 2.62$ cm^3 K mol^{-1}, $C_{obs} = 2.12$ cm^3 K mol^{-1}). These deviations could be due to interactions between Mn^{II} and Mn^{IV} centers or between neighboring Cr^{V} centers or indeed as a result of the small degree on Mn:Cr anti-site disorder. It is however clear that the magnetic moments of all the phases studied are significantly smaller than would be expected if the Mn^{IV} ions in the face-sharing MnO_6 octahedra were acting as simple paramagnetic centers.

Neutron powder diffraction data collected from $Ba_7Mn_5Cr_2O_{20}$ at 5 K in zero applied field can be largely accounted for by a nuclear-only model. Close inspection of this fit reveals broad scattering features which are not accounted for by the structural model, suggestive of short-range magnetic order. Neutron powder diffraction data collected at 5 K from the same sample after field cooling in an applied field of 60 KOe do show diffraction features consistent with magnetic order. The refined magnetic model for $Ba_7Mn_5Cr_2O_{20}$ indicates that the interaction between the Mn^{II} and Mn^{IV} centers (Mn(2) and Mn(3)) is ferromagnetic, as would be expected for a d^5, d^3 180° super-exchange interaction according to the Goodenough−Kanamori rules.[17] The model also shows that the interactions between face-sharing Mn^{IV} centers (Mn(3) and Mn(4)) are antiferromagnetic. This is consistent with analogous structural units in other phases and rationalized by strong direct exchange interactions across the shared faces between MnO_6 octahedra.[18] The combination of ferromagnetic coupling and antiferromagnetic coupling between an odd number of centers (three in this instance) results in a net ferromagnetic moment in each 'chain' of manganese centers.

The lack of 3D magnetic order in zero field can be rationalized by considering the structure of $Ba_7Mn_5Cr_2O_{20}$. Hexagonal perovskites are often considered as being close to one-dimensional materials. The ordering of the manganese and chromium centers and the extensive apex sharing of the B-site polyhedra makes the phases under consideration closer to the two-dimensional limit with sheets of manganese centers separated by a double-layer CrO_4 tetrahedra. Such a model emphasizes the strong magnetic interactions that exist between manganese centers in each sheet and additionally suggests the magnetic coupling between adjacent sheets could be weak as they are separated by two unconnected layers of CrO_4 tetrahedra. On passing through the magnetic ordering transition ~50 K individual layers would become rigorously ordered, but crucially, neighboring layers need not couple so three-dimensional magnetic order is not achieved, and thus, no magnetic Bragg peaks are observed in zero field. Application of an external magnetic field helps to align the net moments in adjacent manganese layers, leading to three-dimensional order. In the presence of two-dimensional magnetic order broad diffraction features arising from the in-plane magnetic lattice are expected as observed in the zero-field 5 K neutron data. The apparent disagreement between the ordered ferromagnetic moment of $Ba_7Mn_5Cr_2O_{20}$ observed by neutron diffraction (4.8 μ_B per f.u.) and directly by magnetometery (7.5 μ_B per f.u.) could be due to a difference in the way the measurements were performed. The

(15) Adkin, J. J.; Hayward, M. A. *Chem. Mater.* **2007**, *19*, 755.
(16) Battle, P. D.; Gibb, T. C.; Jones, C. W. J. *Solid State Chem.* **1988**, *74*, 60–66.
(17) Goodenough, J. B. *Magnetism and the Chemical Bond*; Wiley: New York, 1963.
(18) Daoud-Aladine, A.; Martin, C.; Chapon, L. C.; Hervieu, M.; Knight, K. S.; Brunelli, M.; Radaelli, P. G. *Phys. Rev. B* **2007**, *75*, 104417.

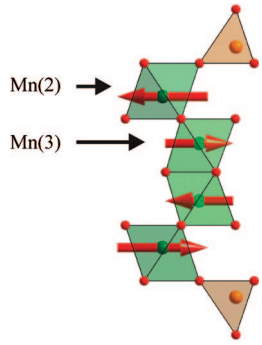

Figure 10. Proposed magnetic coupling scheme for $(Ba_{0.5}Sr_{0.5})_6Mn_4Cr_2O_{17}$.

neutron diffraction data were collected from a tightly packed powder with an isotropic distribution of particle orientations, as confirmed by a lack of preferred orientation in the diffraction data. The magnetization measurements were performed on 'loose' powder samples which were free to reorient on application of the measuring field. In principle, certain particle orientations could prevent or reduce the ability of the applied field to align adjacent magnetic layers. These particles would not contribute to the ordered moment observed by diffraction, leading to the differing values obtained by diffraction and magnetometery.

The magnetic interactions present in $Ba_7Mn_5Cr_2O_{20}$, ferromagnetic 180° super-exchange between d^3 Mn^{IV} and d^5 Mn^{II} and antiferromagnetic direct exchange between Mn^{IV} centers, will also be present in $(Ba_{0.5}Sr_{0.5})_6Mn_4Cr_2O_{17}$. However, replacement of the trimer of face-sharing $Mn^{IV}O_6$ octahedra with a dimer would be expected to yield an antiferromagnetic arrangement as shown in Figure 10. This arrangement would have no net moment, and thus, the ordered manganese layers would not be aligned by application of a field, yielding no magnetic Bragg peaks even in an applied field. Without additional data however it is impossible to be sure this is an accurate description of the magnetic behavior of the six-layer phase as structural features, such as Ba/Sr disorder on the A-site or a degree of manganese charge disorder, offer alternative explanations for the lack of three-dimensional magnetic order.

In conclusion we suggest a model for the magnetic interactions in both $Ba_7Mn_5Cr_2O_{20}$ and $(Ba_{0.5}Sr_{0.5})_6Mn_4Cr_2O_{17}$. Below 300 K (the highest temperature for which we have data) there is strong antiferromagnetic coupling via direct exchange between Mn^{IV} centers in face-sharing MnO_6 units, leading to reduced paramagnetic susceptibilities in the temperature range $100 < T/K < 300$. On cooling to 50 K, ferromagnetic 180° super-exchange interactions between Mn^{IV} and Mn^{II} lead to 2D magnetic order within the sheets of Mn centers. In the case of $Ba_7Mn_5Cr_2O_{20}$, this can be converted into 3D order by application of an external magnetic field.

The complex magnetic behavior observed occurs because there is strong coupling between the different magnetic 'components' which have been rigorously ordered within the host lattice. This ordering is driven by the ability of the different transition-metal coordination sites within the host lattice to differentiate between ions on the basis of both element and oxidation state. This strong differentiation coupled with our growing ability to direct the stacking sequences in anion-deficient hexagonal perovskites suggests these systems are promising hosts for the preparation of new cation-ordered magnetic materials.

Acknowledgment. We thank E. Suard for assistance in collecting the neutron powder diffraction data.

Supporting Information Available: X-ray powder diffraction data collected from $(Ba_{1-x}Sr_x)_7Mn_5Cr_2O_{21-x}$ $(0.3 < x < 0.5)$ samples; observed, calculated, and difference plots and full structural details from the refinements of $Ba_7Ca_2Mn_3Cr_2O_{20}$ and $Ba_7Mn_3V_2O_{20}$; full details of the structural and magnetic refinement of $Ba_7Mn_5Cr_2O_{20}$ at 5 K in an applied field of 60 KOe. This material is available free of charge via the Internet at http://pubs.acs.org.

CM8005138